Article

Sorption Characteristics of Polymer Brushes in Equilibrium with Solvent Vapors

Guido C. Ritsema van Eck,[‡] Lars B. Veldscholte,[‡] Jan H. W. H. Nijkamp, and Sissi de Beer*
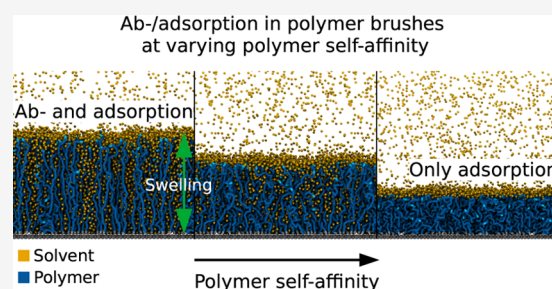
Cite This: Macromolecules 2020, 53, 8428–8437

Read Online

ACCESS | Metrics & More | Article Recommendations | Supporting Information

ABSTRACT: While polymer brushes in contact with liquids have been researched intensively, the characteristics of brushes in equilibrium with vapors have been largely unexplored, despite their relevance for many applications, including sensors and smart adhesives. Here, we use molecular dynamics simulations to show that solvent and polymer density distributions for brushes exposed to vapors are qualitatively different from those of brushes exposed to liquids. Polymer density profiles for vapor-solvated brushes decay more sharply than for liquid-solvated brushes. Moreover, adsorption layers of enhanced solvent density are formed at the brush– vapor interface. Interestingly and despite all of these effects, we find that solvent sorption in the brush is described rather well with a simple mean-field Flory–Huggins model that incorporates an entropic penalty for stretching of the brush polymers, provided that parameters such as the polymer–solvent interaction parameter, grafting density, and relative vapor pressure are varied individually.

Ab-/adsorption in polymer brushes at varying polymer self-affinity

Ab- and adsorption

Swelling

Only adsorption

Solvent
Polymer

Polymer self-affinity

1. INTRODUCTION

When long macromolecules are attached with one end to a surface at a density that is high enough for the polymers to stretch away from the anchoring plane, a so-called polymer brush is formed.[1] Such brushes have many uses.[2] For example, they have been proven to be effective lubricants,[3,4] smart adhesives,[5,6] and sensitive sensors.[7,8] For these applications, the brushes are typically completely immersed in a solvent. However, brushes can also be applied in gaseous environments in equilibrium with a solvent in the vapor phase. This situation is relevant in the context of brushes as model systems of lung tissue,[9] brush-based gas sensors,[10] coatings for moisture management,[11,12] and vapor-solvated lubricants.[13,14] To optimize design parameters for these systems, it is important to understand and characterize vapor sorption in brushes. The interaction between polymer brushes and vapor also has implications for the wetting dynamics of brushes and gel surfaces, another topic of current interest.[15–17] In many experimental studies of vapor sorption in polymer brushes, the Flory–Huggins theory[18] for polymer–solvent mixtures is employed to model the solvent's volume fraction in the brush as a function of the relative vapor pressure.[19–22] Under the condition that the solvent vapor is in chemical equilibrium with the solvent in the polymer–solvent mixture, a prediction of the brush composition is obtained. Although this theory is useful for describing qualitative trends, it fails to capture brush-specific effects. In its simplest form, application of the Flory– Huggins theory leads to the assumption of a homogeneous density of solvent throughout the brush. However, neutron reflectometry measurements of vapor-solvated brushes indicate that the brush density decreases as a function of the distance

from the anchoring surface.[23] Another assumption in the basic Flory–Huggins model is that brush swelling is independent of the grafting density, while experimentally, it is found that the swelling increases with decreasing grafting density.[24] A model that includes the entropic penalty for polymer stretching allows for predicting grafting density effects, even in a mean-field approach.[24,25] A third assumption in the basic Flory–Huggins model is that it accounts for the polymer–solvent interactions via a single Flory–Huggins parameter χ_{ps}. Thereby, inter- actions of polymers and solvent with air are assumed to be equal and interfacial effects are not captured in the model. Yet, neutron reflectometry measurements indicate the existence of a solvent-enriched layer at the brush–air interface,[21,23] even though the authors of ref 21 considered their density variation to be a fitting artifact. Therefore, the question arises if the employment of a Flory–Huggins-type model is appropriate for vapor-solvated brushes.

In this article, we use molecular dynamics (MD) simulations to provide a detailed microscopic interpretation of solvent sorption for polymer brushes in equilibrium with solvent vapors for different interaction parameters, brush densities, and relative solvent pressures. We evaluate the polymer and solvent density profiles and discuss similarities and differences with the
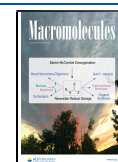
profiles for brushes in contact with liquids as well as experimental observations. Moreover, we compare the solvent fraction in our brushes to a modified Flory–Huggins model, to investigate the validity of Flory–Huggins-type models for systems containing solvent vapors. Solvent adsorption at the brush–vapor interface is quantified across the parameter space of interaction energies as well and discussed in the context of predictions based on energetic arguments.

2. MODEL AND METHODS

Solvent partitioning is investigated using coarse-grained molecular dynamics (MD) simulations of the brush–solvent system, alternated with grand-canonical Monte Carlo (GCMC) sweeps to maintain a constant solvent vapor pressure in a region above the brush. In this GCMC procedure, a set number of particle insertions and deletions is attempted and evaluated based on a Metropolis criterion. All simulations were performed using the MD package large-scale atomic/molecular massively parallel simulator (LAMMPS).[26]

A system is set up consisting of a rectangular box of dimensions 50 × 50 × 100 σ^a (x, y, z, respectively) that is periodic in x and y. Polymer chains are represented by a freely jointed bead–spring model based on the work of Kremer and Grest,[27] and consist of N = 30, 60, or 100 beads each. These lengths are selected to limit computational costs while still producing the characteristic behaviors of polymers.[14,28] We note that our brushes are perfectly monodisperse. Polydispersity can qualitatively alter density profiles, penetration,[29] and absorptive properties.[30] Therefore, we anticipate that our results might change when polydispersity is introduced. A polymer brush is created by "grafting" chains to immobile particles positioned randomly in a plane at the bottom of the box (z = 0). The code used to generate the initial data comprising these polymer brush systems is available online.[31] Above the polymer brush at the top of the box, solvent particles are inserted/removed in a 20 σ thick slab according to the GCMC procedure outlined above, as illustrated in Figure 1. The background medium (air) is modeled implicitly. A
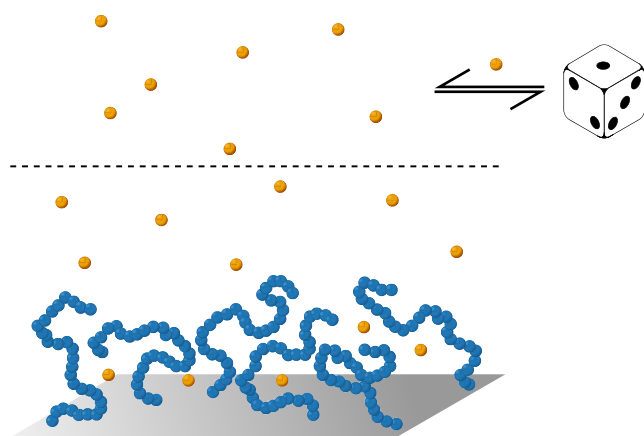

Figure 1. Schematic of the simulation box. Monodisperse polymer chains of length N = 30 are grafted to an atomic wall to form the brush. Above the brush, a vapor region periodically exchanges particles with a virtual reservoir through the GCMC procedure.

system of low-density Lennard-Jones (LJ) particles in an implicit background is similar to simulations of brushes in contact with nanoparticles[32] or co(non)solvents,[33] except that our implicit background is a poor solvent for the brushes. Repulsive harmonic 'mathematical walls', with a spring constant of 100 $\epsilon\sigma^{-2}$,[a] are placed at the bottom and top of the box to prevent polymer and vapor particles from leaving the system through the fixed boundary in z.

Nonbonded interactions in the system are described by a form of the well-known Lennard-Jones (LJ) potential

$$U_{LJ}(r) = 4\epsilon\left(\left(\frac{\sigma}{r}\right)^{12} - \left(\frac{\sigma}{r}\right)^6\right) \tag{1}$$

where r represents the interparticle distance, ϵ is the depth of the potential well, and σ is the zero-crossing distance. The minimum occurs at $r_m = 2^{1/6}\sigma$. Specifically, the truncated and potential-shifted (SP) form of the Lennard-Jones potential is used

$$U_{LJ,SP}(r) = \begin{cases} U_{LJ}(r) - U_{LJ}(r_c) & \text{for } r \leq r_c \\ 0 & \text{for } r > r_c \end{cases} \tag{2}$$

where r_c is the cutoff distance for the interaction. Throughout this work, we use reduced Lennard-Jones units, meaning that ϵ and σ are used as energy and length units for our system, respectively. Additionally, all particle masses are equal. All of these interactions are truncated and potential-shifted to zero at 2.5 σ. Therefore, all interparticle interactions in our simulations are attractive at distances larger than 1 σ. Consecutive beads along a polymer backbone are bonded via a finitely extensible nonlinear elastic (FENE) potential (eq 3) combined with a Weeks–Chandler–Anderson (WCA) potential (eq 4). The latter is equivalent to an LJ potential truncated at its minimum and shifted to zero at the cutoff, thereby making it purely repulsive. The total bonded potential is the sum of the FENE and WCA potentials (eq 5).

$$U_{FENE}(r) = -0.5KR_0^2 \ln\left(1 - \left(\frac{r}{R_0}\right)^2\right) \tag{3}$$

$$U_{WCA}(r) = \begin{cases} U_{LJ}(r) + \epsilon & \text{for } r \leq 2^{1/6} \\ 0 & \text{for } r > 2^{1/6} \end{cases} \tag{4}$$

$$U_{bond}(r) = U_{WCA}(r) + U_{FENE}(r) \tag{5}$$

In eq 3, R_0 is the maximum bond length and K is a spring constant. In our simulations, K is set to 30 $\epsilon\sigma^{-2}$, R_0 is 1.5 σ, and ϵ and σ are equal to 1. These parameters, borrowed directly from the Kremer–Grest model,[27] prevent bond crossing and other unphysical behaviors. This model evidently cannot account for various chemical specificities. In particular, the effects of molecular geometry and directional interactions such as hydrogen bonding cannot be captured effectively by a Lennard-Jones-based model. Our results will therefore deviate somewhat from those of most experimental systems. However, that same generality makes this simulation setup particularly suitable for testing the applicability of the extended Flory–Huggins model to vapor sorption.

The entire system is thermostatted to a temperature of 0.85 ϵk_B^{-1} using a chain of three Nosé–Hoover thermostats (which ensures proper sampling of the canonical ensemble[34]) with a damping constant of 0.15 τ, where τ represents the reduced time unit derived from the Lennard-Jones potential. k_B is the Boltzmann constant, which we take to be unity, as the energy scale of the simulations is arbitrary. The temperature of 0.85 ϵk_B^{-1} was determined to allow vapor–liquid coexistence for the solvent. The GCMC chemostat is active every 10 000 time steps, where it attempts 1000 solvent particle insertions/deletions. These values were empirically determined to result in a good balance between simulation performance and convergence speed.

The polymer system is first equilibrated by running a short minimization using the conjugate gradient method, followed by running dynamics for 10 000 time steps with a limit imposed on the maximum movement of a particle in one time step of 1 σ and a Langevin thermostat with a damping parameter of 1000 τ. A second minimization is then performed. Finally, 200 000 time steps of more viscous Langevin dynamics are performed with a damping parameter of 100 τ and without the limit. This procedure is chosen to relax the system from the low-entropy initial state (fully extended chains) as quickly and efficiently as possible. After the equilibration, a production run is started in which solvent particles are introduced

into the system by enabling the GCMC mechanism. The system is simulated for 60 million time steps (900 000 τ), as this ensures an equilibrated state and adequate signal-to-noise ratio for all simulation cases. LAMMPS input files as well as a Python wrapper around LAMMPS are available online.[35]

For the equilibration, the LAMMPS default value for the time step (0.005 τ) is used. For the production runs, the rRESPA multi-time-scale integrator[36] is employed with an outer time step of 0.015 τ and a twofold shorter inner time step. This results in nonbonded pair interactions being computed every 0.015 τ, but bonded interactions being computed every 0.0075 τ.

The depth of the energetic minimum of the polymer self-interaction (ϵ_{pp}) and of the polymer−solvent interaction (ϵ_{ps}) are both varied with the goal of identifying sorption behavior regimes of the vapor-solvated polymer brush system in the two-dimensional parameter space. We assume the ϵ values to represent general short-range interactions and therefore do not account for combining rules in our selection of parameter space. For solvent self-interactions, we use the reference value of unity for ϵ. In our primary simulations, the GCMC chemostat maintains a solvent pressure of 0.0154 $\epsilon\sigma^{-3}$, corresponding to a relative pressure of $P/P_{sat} \approx 0.73$. Simulations are performed for brush systems with average grafting densities of 0.34 σ^{-2} (in the case of $N = 30$), and 0.15 and 0.25 σ^{-2} (in the case of $N = 100$). These values are chosen so that the mean distance between polymers is significantly smaller (up to an order of magnitude) than the radius of gyration for a collapsed single chain. This ensures brush conditions in the full range of solvent conditions probed and prevents the formation of octopus micelles[37] under poor solvent conditions, which was observed at lower grafting densities. Radii of the collapsed chains were determined through long single-chain simulations of free polymers with a poor implicit medium. Additionally, the solvent pressure is also varied from 0.0021 $\epsilon\sigma^{-3}$ to 0.0208 $\epsilon\sigma^{-3}$ (corresponding to relative pressures from 10 to 99%) at constant ϵ_{pp} and ϵ_{ps}.

The sorption behavior of the system is evaluated by analyzing density profiles of the polymer and the solvent over the z direction (averaged over x and y). During the simulation, these are dumped every 10 000 time steps (averaged over 100 time steps equally spaced out since the previous frame). To ensure properly equilibrated results, the first 95% of all frames are discarded and only the last 5% are time-averaged for further processing. For the calculation of several physical quantities, definitions of spatial limits are required. First, the brush height is defined by the inflection point (point of maximum slope, as determined using a Savitzky−Golay filter) in the polymer density profile. Second, we define an outer limit for the adsorption layer by an (arbitrary) lower threshold of 0.002 σ^{-4} in the solvent density gradient. Any solvent beyond this point is considered vapor bulk. To mitigate discretization errors in the determination of the limits described above, the density profiles are spatially interpolated 10 times using a cubic spline interpolant prior to time-averaging. The amount of absorption (solvent inside the brush) is calculated as the integral of the solvent density profile up to the brush height, and similarly, the amount of adsorption is calculated as the integral of the solvent density profile from the brush height up to the adsorption layer end. The Python code that implements this procedure is available online.[38]

3. THEORY

The interaction between solvents and grafted or adsorbed polymers is often described using the Flory−Huggins model of mixing.[39−41] The Flory−Huggins model is a lattice model, in which every particle is assumed to occupy exactly one site in a fully occupied lattice of arbitrary geometry.[42] Polymer beads and solvent particles are placed onto lattice sites randomly, respecting the requirement of connectivity along polymer backbones. Employing a mean-field assumption with respect to the composition of the system, the combinatorial entropy of

placing the particles on the lattice can be determined, resulting in an entropy-of-mixing expression

$$\frac{\Delta S_{mix}}{k_B} = -(n_s \ln \phi_s + n_p \ln \phi_p) \tag{6}$$

with S being the entropy, n the number of molecules of a given species, ϕ the site fraction of a given species, and subscripts s and p denoting the solvent and the polymer, respectively. Note that n_p represents the number of polymer chains and so the number of polymer-occupied sites is $n_p N$, with N being the degree of polymerization. The energetic effects of mixing are treated by defining an interaction parameter

$$\chi = \frac{zW}{k_B T} \tag{7}$$

where z is the coordination number of the lattice, T is the temperature, and W is the energetic effect of forming a single solvent−polymer contact by eliminating solvent−solvent and polymer−polymer contacts, meaning that

$$W = -\epsilon_{ps} + \frac{1}{2}(\epsilon_{ss} + \epsilon_{pp}) \tag{8}$$

under the assumption that the spacing of the Flory−Huggins lattice is determined exactly by the minimum of the Lennard-Jones potential. Hence, negative W indicates that mixing is enthalpically favorable, although entropy-driven mixing may still be possible for positive W. We will refer to W as the relative affinity between the polymer and the solvent.

Using the aforementioned mean-field assumption for the polymer and solvent concentrations, this results in an energetic contribution of

$$\frac{U_{mix}}{k_B T} = \chi n_s \phi_p \tag{9}$$

and total free energy of mixing of

$$\frac{F_{mix}}{k_B T} = n_s \ln \phi_s + n_p \ln \phi_p + \chi n_s \phi_p \tag{10}$$

The model as outlined above does not account for grafting effects, however. First of all, grafting of the polymer chains removes their translational entropy, meaning that the second addend in eq 10 should be eliminated. Additionally, grafted chains can swell only by extending, which incurs an entropic penalty. A mean-field elasticity term dependent on the height of the brush can be used to describe the entropic elasticity of polymer chains in the swollen brush.[24,43] This requires $\rho_g \ll N^{2/3}$ (with ρ_g being the grafting density of the brush in chains σ^{-2}), as this ensures that collapsed brush states do not display substantial lateral inhomogeneities.[43] Our primary simulations meet this condition by a factor of roughly 3.5. The introduction of this elasticity results in a new free-energy expression

$$\frac{F_{mix}}{k_B T} = n_s \ln \phi_s + \chi n_s \phi_p + n_p \frac{3h^2}{2N} \tag{11}$$

with h being the height of the polymer brush. This amounts to an Alexander−De Gennes ansatz,[44,45] in which all chain ends are located at the outer edge of the brush. Assuming the density of the swollen brush to be independent of its composition, the height of the brush becomes directly
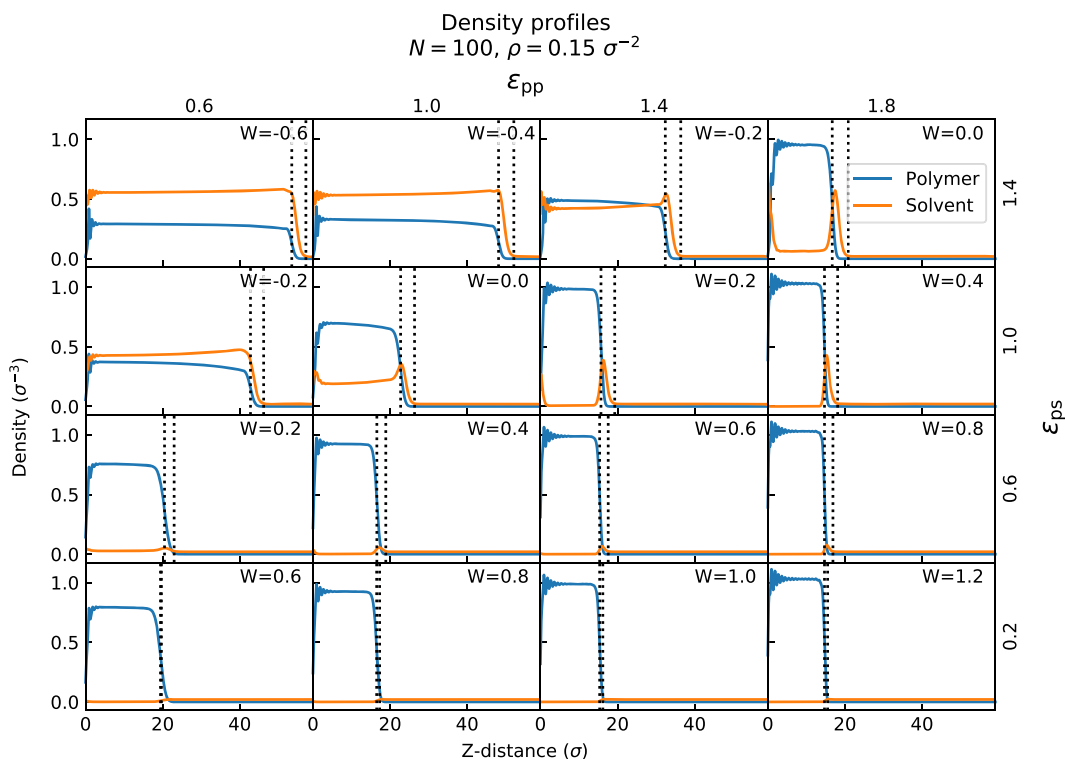
Figure 2. Density profiles of polymer (blue) and solvent (orange) for a 4 × 4 grid of ϵ_{pp} and ϵ_{ps} values, at $N = 100$ and $\rho = 0.15\ \sigma^{-2}$. The dotted lines indicate the limits of the adsorption layer as defined by the top of the polymer brush and the top of the adsorbed solvent layer, respectively.

proportional to the number of particles per unit area. Per polymer chain, this may be expressed as

$$h \approx \frac{N\rho_g}{\phi_p} \tag{12}$$

As a result, the elasticity term can also be expressed in the form

$$n_p \frac{3N\rho_g^2}{2\phi_p^2} \tag{13}$$

Taking the derivative of this elasticity-adjusted free-energy expression with respect to the amount of absorbed solvent yields the chemical potential for the solvent within the brush

$$\frac{\mu_{in}}{k_B T} = \ln(1 - \phi_p) + \phi_p + \chi\phi_p^2 + \frac{3\rho_g^2}{\phi_p} \tag{14}$$

Note that any direct dependence on N can be incorporated into a ϕ_p term, meaning that we expect to see a quantitatively similar relation between interaction parameters and bulk composition for different chain lengths. Although this is convenient for the current discussion, this prediction is limited to monodisperse systems, as it relies on the assumption that every polymer chain occupies the same volume.

At chemical equilibrium, the chemical potentials for the solvent inside the brush and for the solvent vapor phase are equal by definition. Ideally, the chemical potential of the bulk vapor is given by

$$\frac{\mu_{out}}{k_B T} = \ln\left(\frac{P}{P_{sat}}\right) \tag{15}$$

with P indicating the pressure of the vapor phase and P_{sat} indicating the saturation pressure of the vapor. We outline a procedure for determining P_{sat} of the simulated vapor in the Supporting Information (SI), Section S1. Hence, the equilibrium absorption behavior of the brush is determined by

$$\ln\left(\frac{P}{P_{sat}}\right) = \ln(1 - \phi_p) + \phi_p + \chi\phi_p^2 + \frac{3\rho_g^2}{\phi_p} \tag{16}$$

From this, we obtain dependencies of the brush swelling on several parameters. The absence of explicit dependencies on the individual interaction energies ϵ_{ss}, ϵ_{pp}, and ϵ_{ps} indicates that we may expect identical sorption behavior for any combination of interaction energies that results in a given value of χ. It should be noted that this is reliant on the assumption that the system density and coordination number remain constant with this variation of interaction energies, however.

Since Flory–Huggins-derived models are primarily concerned with bulk composition, we may expect the greatest deviation from conventional theory at the brush–vapor interface. Both the structure and the composition of the interface are not easily predicted. However, by describing the system as sharply defined polymer, solvent, and vapor layers, we can obtain a first approximation of the adsorption behavior. In this idealized model, adsorption would be determined by the Hamaker constant for polymer and vapor interacting across the solvent layer.[46] Making use of combining rules, the Hamaker constant for such a three-phase system can be decomposed into the Hamaker constants for individual materials in vacuum as

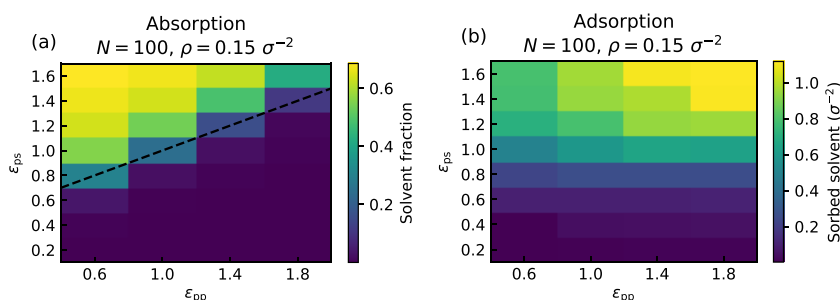$$A_{psv} = \left(\sqrt{A_{pp}} - \sqrt{A_{ss}}\right)\left(\sqrt{A_{vv}} - \sqrt{A_{ss}}\right) \tag{17}$$

Figure 3. Heatmaps of the amount of absorption (solvent fraction) (a) and adsorption (integrated solvent density) (b) at $N = 100$ and $\rho = 0.15$ σ^{-2}. The dashed line in the absorption heatmap denotes the locus where $W = 0$.

with A being the Hamaker constant and the subscript v denoting vapor. If this combined Hamaker constant is negative, the net interaction between the polymer–solvent and solvent–vapor interfaces is repulsive, meaning that the formation of an adsorption layer is energetically favorable. A_{ii}, with i being an arbitrary component, is typically positive, and is negligible for gases. Hence, the second term on the right-hand side of eq 17 will always be negative for the systems under consideration, and the sign of A_{psv} is determined by the first term. Under the simplifying assumption that the polymer and solvent phases are entirely incompressible (i.e., their density is independent of their self-affinity), A_{pp} and A_{ss} become directly proportional to ϵ_{pp} and ϵ_{ss}. As a result, we may expect adsorption for $\epsilon_{pp} > \epsilon_{ss}$. Note, however, that this approach implicitly assumes no absorption of the solvent, and makes use of the same mixing rules we explicitly disregard in our parameter selection.

4. RESULTS AND DISCUSSION

In this section, we will first discuss the effects of the individual interaction energies ϵ_{pp} and ϵ_{ps} on sorption behavior, based on density profiles extracted from our simulations. We also discuss the effect of the relative polymer–solvent affinity W and relate this to the Flory–Huggins theory. Next, we show results across the same parameter space for different brush densities and compare brush density effects to theory. Finally, we show the effect of the relative vapor pressure on absorption for selected interaction energies, at chain lengths of $N = 30$, 60, and 100. Data underlying all figures are available online free of charge.[47]

It is typical to discuss interactions in polymeric systems in terms of a second virial coefficient, as seen in related work by Mukherji et al.[48] and Opferman et al.[49] We express our results in terms of W and various ϵ since this work is restricted to particles of a single size. A model for the general case would have to make use of such a virial coefficient to account for particle size effects.

4.1. Effect of Brush and Solvent Affinities. The density profiles obtained for a 4x4 grid in the ϵ_{pp}, ϵ_{ps} parameter space are shown in Figure 2. Each of the 16 graphs shows the density profiles (number density vs z-distance) of the polymer (blue) and solvent (orange) particles in the brush system. The polymer brush height is indicated by the first dotted vertical line. The second dotted line indicates the outer edge of the adsorption layer.

Immediately visible is absorption in the top-left corner of Figure 2 (low ϵ_{pp}, high ϵ_{ps}) indicated by the elevated concentration of the solvent within the brush. In contrast, in the top-right corner (high ϵ_{pp}, high ϵ_{ps}), solvent uptake is dominated by adsorption, as shown by the peaks in solvent density near the brush surface. Little sorption of any kind

occurs at the lower part of the figure (low ϵ_{ps}). Note that adsorption and absorption are not mutually exclusive, as evidenced by the coexistence of bulk absorption with a solvent density peak at the interface at several points (e.g., $\epsilon_{pp} = \epsilon_{ps} = 1.4$).

In the absorption regime (top left of Figure 2), we observe solvent uptake coupled with strong swelling of the brush, as well as the formation of a solvent layer on top of the brush. Taking the dry brush height at a given ϵ_{pp} as a reference, we find swelling ratios of over 2 for the most swollen systems. This is comparable to experimentally determined swelling ratios, which range up to approximately 2 for poly(methyl methacrylate),[24] modified poly(2-(dimethylamino)ethyl methacrylate),[22] and poly(2-methacryloyloxyethyl phosphorylcholine)[50] brushes under good solvent vapors. Polymer density profiles decay only very slightly as a function of the distance from the surface and then fall off dramatically in a narrow interfacial region. This behavior qualitatively resembles the results of a self-consistent field model by Sun et al.[23] This model predicts polymer brushes under a vapor atmosphere to assume a density profile similar to the classical parabolic field,[1,51] but with a more sharply defined interface. Furthermore, solvent densities in these highly swollen systems are generally high and constant throughout the brush. This suggests that the attraction between the polymer and the solvent leads to condensation of the vapor. The occurrence of absorption for these parameter combinations matches a simple picture based on the interchange energy between bulk phases. As the insertion of a solvent particle into the brush leads to the displacement of polymer–polymer interactions, the polymer–solvent affinity must be greater than the average of the polymer and solvent self-affinities for absorption to occur.

As we move to the top-right corner of the figure, we observe primarily adsorption, as the strong polymer self-affinity largely precludes solvent absorption; the interior of the polymer brush contains little to no solvent, but a solvent layer still covers the surface of the brush. Translational entropy of the solvent leads to some penetration of the solvent into the brush, but chain stretching into the solvent layer is precluded by the associated entropic penalty. As a result, the brush density profile falls off rather sharply near the interface in this regime. The fact that an adsorption layer of the solvent can form for a wide range of interaction parameters is notable. Liquid adsorption on polymer brushes is of great practical interest, as, e.g., the lubricious properties of brushes result in significant part from the formation of a stable liquid layer on top of the brush.[40,52] We also find enrichment in the solvent near the grafting plane in a number of these systems. Since the grafting plane truncates the brush bulk, it creates a second interfacial region. We may

therefore expect the component that interacts less strongly with the bulk to accumulate at the grafting plane. The adsorption of the solvent to the grafting plane is further favored by the fact that the solvent monomers do not lose any conformational entropy near the grafting plane, unlike the polymer chains.

Finally, the bottom profiles (low ϵ_{ps}) exhibit little sorption at all. W values in this regime are positive or zero, and solvent absorption carries an entropic penalty through chain stretching. As previously discussed, we would still expect adsorption for the cases where $\epsilon_{pp} > \epsilon_{ss}$, as this results in a negative value of the two-interface Hamaker constant. However, ϵ_{ps} is also less than $k_BT = 0.85$, meaning that the thermal motion of the solvent particles will dominate over the polymer–solvent attraction. A stable adsorption layer cannot be formed as a result. For $\epsilon_{ps} = 0.6$ and $\epsilon_{pp} = 0.6$, the small adsorption appears to be inside the brush. However, examination of the snapshots indicates that the solvent resides to a large extent in valleys of the rough brush surface, instead of inside the brush.

Figure 3a,b show heatmaps of the solvent fraction inside the brush and the integrated excess solvent density outside of the brush, respectively, over the ϵ_{pp}, ϵ_{ps} space covered by our simulations. From Figure 3, it is clear that both adsorption and absorption vary with ϵ_{pp} as well as ϵ_{ps}.

Absorption appears to be approximately constant along lines of slope 1/2. Since the solvent self-affinity for these systems is fixed, this corresponds to constant W. This indicates that mixing behavior is determined by the relative polymer–solvent affinity, and may follow the Flory–Huggins theory. We discuss this point in more detail further on.

In the diagram for adsorption, a sharp increase in adsorption is clearly visible between $\epsilon_{ps} = 0.8$ and 1, corresponding to the requirement that $\epsilon_{ps} > k_BT$. Adsorption increases with ϵ_{pp}, matching our previous argument based on the Hamaker constant. More intuitively, this behavior can also be explained as a density effect. For strong polymer self-affinities, the attraction between beads leads to relatively dense, contracted brush profiles. As a result, the density of attractive interactions that a solvent particle near the interface experiences will increase with ϵ_{pp}, rendering adsorption more favorable energetically. Moreover, for lower ϵ_{ps}, solvent absorption increases, such that polymer density at the top of the brush reduces even further.

At high ϵ_{ps}, some degree of solvent adsorption persists even when $\epsilon_{pp} < \epsilon_{ss}$, contradicting our expectations based on the two-interface Hamaker constant. The observation of an enhanced solvent density at the top of the brush for highly swollen brushes is consistent with experimental observations.[21,23] Yet, it appears to clash with the self-consistent field theory by Cohen Stuart et al.,[53] which indicates the possibility of chain segments adsorbing at the brush–air interface for low ϵ_{pp}. We attribute the absence of a polymer-enriched phase at the interface to the relatively high entropic penalty for chain stretching, which arises from the relatively short chain length and high grafting density we employ in our simulations. This is supported by polymer and solvent density profiles for $N = 30$, presented in the SI (Section S3). In these profiles, the difference between solvent densities in the brush bulk and at the interface is more pronounced than that for $N = 100$, suggesting that the finite extensibility of the polymer chains does indeed limit polymer adsorption at the interface. We intend to study this in more detail in future work.

Figure 4 presents the same information as Figure 3a, but in the form of a solvent fraction against W, which represents the
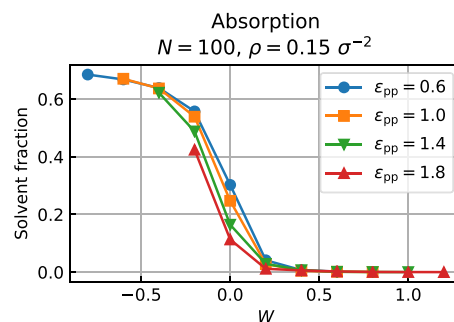

Figure 4. Absorption (solvent fraction) plotted against the relative affinity W for several values of ϵ_{pp}, at $N = 100$ and $\rho = 0.15$. The lines connecting markers are meant to guide the eye.

energetic effect of forming a single polymer–solvent contact at the expense of the polymer and solvent bulk interactions. Conventionally, W is expected to be directly proportional to χ (see eq 7). For all values of ϵ_{pp}, the transition from a collapsed brush to a swollen one occurs in the same range of W values, with higher ϵ_{pp} showing less absorption in the intermediate range. For all ϵ_{pp}, absorption is observed for positive W already, where interaction energies alone are not sufficient to result in mixing. This indicates that the increase in translational entropy for our solvent beads is higher than the entropic penalty for polymer stretching upon mixing these concentrations. The opposite is often observed for brushes in contact with polymer melts[54−56] because melt polymers gain less translational entropy than solvent molecules upon mixing.

The relatively minor difference in the transition W is remarkable, as the relative affinity is defined between two dense bulk phases. No liquid solvent bulk phase is present in our simulations, however. In a simple view of the system, this would lead us to expect a negligible effective value for ϵ_{ss} due to the low density of the vapor phase, and a free energy of mixing dependent on the composition of the interface. We speculate that vapor absorption in polymer brushes is a two-step process, in which particles are first adsorbed to form a dense (multi-)layer, which subsequently diffuses into the polymer phase. A more detailed examination of the evolution of the system will be addressed in future work.

Despite qualitative similarities, the absorption behavior for different ϵ_{pp} in Figure 4 varies quantitatively at intermediate values of W. Specifically, systems with a low polymer self-affinity absorb more solvent. This is possibly because dry brushes at high self-affinity are denser than their low-ϵ_{pp} counterparts (see Figure 2, bottom row). If free volume is present in the dry brush, the free site may be replaced with a solvent particle at no cost of combinatorial entropy and without increasing the brush stretching. Hence, a brush that contains free volume in its dry state incurs a smaller entropic penalty for absorbing moderate amounts of solvent. This also matches the fact that solvent fractions appear to tend toward a common plateau value again at very negative W. This does represent a breakdown of the assumption that the polymer phase is incompressible, which we have used so far. In the context of the extended Flory–Huggins model, this would have two consequences: with a change of the interparticle distance, the effective strength of interactions between neighboring particles would also change, and the coordination

number (z in eq 7) in the fluid would no longer be constant. The latter, in particular, could have a substantial impact on system behavior. The former is of less concern, as the ϵ values we choose remain linearly related to the actual interaction.

A dependence of the coordination number on ϵ_{pp} would provide an intuitively attractive explanation for the difference in absorption across the transition shown in Figure 4. However, if this were the case, we would expect to see equal solvent fractions for all systems at $W = 0$, since this corresponds to an χ value of 0 regardless of the coordination number. While it is plausible that z would vary with ϵ_{pp}, we consider it unlikely that this would be the sole cause of the variation in absorption. We also note that the shape of the absorption curves appears to vary, suggesting either a nonlinear relation between ϵ_{pp} and the effective interaction parameter or dependence on ϵ_{ps} as well as ϵ_{pp}. In SI Section S4, we display the calculated χ values based on the solvent fraction for each point in Figure 4.

4.2. Effect of Grafting Density.
Figure 5 displays the amount of absorbed solvent as a function of W for two
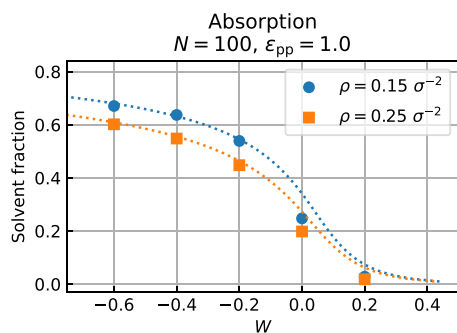

Figure 5. Absorption (solvent fraction) plotted against the relative affinity W for two different grafting densities at $N = 100$ and $\epsilon_{pp} = 1.0$. The dotted curves correspond to theoretical predictions.

different values of the grafting density. Theoretical curves were obtained by rearranging eq 16 to isolate χ. A linear relation between χ and W was obtained through a least-squares fit for the calculated χ of all points of $\epsilon_{pp} = 1.0$ in Figure 4. As we discussed already, W and the effective χ may not be directly proportional.[57] Yet, we consider this approach more informative than ad hoc adjustments. As the relative affinity becomes positive, both curves tend toward zero absorption. For strongly negative values of W, solvent fractions at both grafting densities tend toward a plateau value, as the brush becomes saturated with the solvent. These plateau values must decrease with grafting density for a given chain length, as the maximum volume available to the brush depends only on the chain length. Below these plateau values, the brush of lower grafting density still takes up more solvent. This matches the extended Flory–Huggins model: the elasticity contribution to the free energy (eq 11) is quadratic in h, and h is directly proportional to the number of particles under the assumption that the brush–solvent system is incompressible. Hence, the chemical potential for solvent particles in the brush will be more positive in a more extended brush, i.e., the one with higher grafting density (all else remaining equal).

4.3. Effect of Relative Vapor Pressure.
Solvent fractions in the brush as a function of the relative solvent pressure are depicted in Figure 6 for three different polymer chain lengths
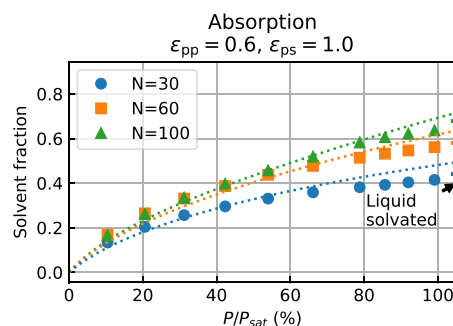

Figure 6. Absorption (solvent fraction) plotted against the relative solvent vapor pressure for different chain lengths, at $\epsilon_{pp} = 0.6$ and $\epsilon_{ps} = 1.0$. The grafting densities used are $\rho = 0.34$, 0.21, and 0.15 σ^{-2}, respectively (for increasing N). The dotted curves correspond to theoretical predictions for $\chi = -1.7$.

at $\epsilon_{pp} = 0.6$, $\epsilon_{ps} = 1.0$. We obtain an expected pressure–composition relation by exponentiating eq 16, resulting in

$$\frac{P}{P_{sat}} = (1 - \phi_p)\exp\left(\phi_p + \chi\phi_p^2 + \frac{3\sigma^2}{\phi_p}\right) \tag{18}$$

We realize that ϕ_p results from the imposed $\frac{P}{P_{sat}}$. Yet, we express $\frac{P}{P_{sat}}$ in terms of ϕ_p rather than vice versa because the resulting expression is more convenient to work with. In experiments and simulations, the relative solvent pressure will generally be the independent variable, and the model discussed thus far depends on the vapor phase being unaffected by the brush composition. In a traditional Flory–Huggins description, ϕ_p would go to zero as $\frac{P}{P_{sat}}$ approaches unity. However, this causes the elasticity term $\frac{3\sigma^2}{\phi_p}$ to diverge, and we obtain a finite ϕ_p when $\frac{P}{P_{sat}} = 1$. The theoretical curves displayed correspond to an χ parameter of -1.7, which was determined based on a least-squares fit of the data for $N = 100$. In accordance with the extended Flory–Huggins model, we find that the solvent fraction increases nonlinearly with the relative solvent pressure, and reaches a plateau value at high $\frac{P}{P_{sat}}$. This indicates that the presence of the brush cannot cause the condensation of a macroscopic solvent layer. For low values of $\frac{P}{P_{sat}}$, the expected absorption curves closely match the observed absorption behavior. At higher relative pressures, however, the solvent fraction as extracted from our simulations levels off more than expected. This may once again be an effect of finite chain extensibility. Absorption behavior is qualitatively the same for all cases but varies quantitatively with the chain length. This can be attributed to the difference in grafting density between systems, as the absorption behavior described by eq 18 does not depend directly on the polymer chain length.

Experimental results show typical curves of absorption against pressure to be convex,[19−22,25,58] as opposed to the concave relations we obtain from both theory and simulations. This difference in the shape of the absorption curve is a consequence of the large negative value of χ and the high grafting density of the brush. For positive χ, the extended Flory–Huggins model does indeed predict the absorption curve to be convex. Predicted pressure–composition relations

for a range of values are presented in Section S5 of the SI. Flory−Huggins parameters for well-solvated polymers are typically close to 0.5, although small negative values of χ are experimentally attainable.[59] This suggests that it may be possible to realize such concave−downward absorption curves experimentally for a highly attractive solvent−brush combination at high grafting densities. As such a system would retain large amounts of solvent even at low partial solvent pressures, this could increase the longevity and robustness of specific brush−solvent systems in air.

5. CONCLUSIONS

Solvent absorption and adsorption for polymer brushes in chemical equilibrium with solvent vapor have been investigated for a range of interaction parameters, brush densities, and relative solvent pressures. The densities for brushes and solvents for vapor-solvated systems are different from the density profiles for liquid-solvated systems. Moreover, adsorption films with an enhanced solvent density can be observed. Via analysis of the solvent fraction in the brushes, we find that a Flory−Huggins model that incorporates an entropic penalty for stretching brush polymers describes highly swollen systems at different grafting densities well, but appears to overestimate absorption for high relative solvent pressures and in the onset of absorption. Variation of interaction parameters indicates that the effective value of χ depends on individual interaction parameters even in the absence of chemical specificity. This is a departure from the classical definition of the Flory−Huggins parameter as a function of the interchange energy between two components. The occurrence of adsorption is predicted qualitatively by the classical Hamaker theory, independently of the absorption behavior. However, some nonidealities are seen as a result of differences in the composition of the brush−air interface and the finite length of the simulated polymers. To further improve Flory−Huggins-type models, chain conformations and free volume in the brush as a function of the interaction energies should be investigated.

■ ASSOCIATED CONTENT

Ⓢ Supporting Information

The Supporting Information is available free of charge at https://pubs.acs.org/doi/10.1021/acs.macromol.0c01637.

> Discussion of the procedure used to obtain values of P_{sat} of the Lennard-Jones vapor; discussion of the relation between P and P_{res}; density profiles of polymer brushes under vapor at chain length $N = 30$; plot of the effective values of the χ parameter obtained from our simulations; and plot of the predicted absorption behavior against relative solvent pressure for various values of χ (PDF)

■ AUTHOR INFORMATION

Corresponding Author

Sissi de Beer − *Materials Science and Technology of Polymers, University of Twente, Enschede 7522 NB, The Netherlands;* ◉ orcid.org/0000-0002-7208-6814; Phone: +31 (0)53 489 3170; Email: s.j.a.debeer@utwente.nl

Authors

Guido C. Ritsema van Eck − *Materials Science and Technology of Polymers, University of Twente, Enschede 7522 NB, The Netherlands*

Lars B. Veldscholte − *Materials Science and Technology of Polymers, University of Twente, Enschede 7522 NB, The Netherlands;* ◉ orcid.org/0000-0002-2681-2483

Jan H. W. H. Nijkamp − *Materials Science and Technology of Polymers, University of Twente, Enschede 7522 NB, The Netherlands*

Complete contact information is available at:
https://pubs.acs.org/10.1021/acs.macromol.0c01637

Author Contributions

[‡]G.C.R.v.E. and L.B.V. contributed equally to this work.

Notes

The authors declare no competing financial interest.

■ ADDITIONAL NOTE

[a]Where σ and ϵ are the length and energy unit (respectively) in the system of reduced Lennard-Jones units used in this work.

■ REFERENCES

(1) Milner, S. T. Polymer brushes. *Science* **1991**, *251*, 905.

(2) Chen, W.-L.; Cordero, R.; Tran, H.; Ober, C. K. 50th Anniversary Perspective: Polymer Brushes: Novel Surfaces for Future Materials. *Macromolecules* **2017**, *50*, 4089−4113.

(3) Klein, J.; Kumacheva, E.; Mahalu, D.; Perahia, D.; Fetters, L. J. Reduction of frictional forces between solid surfaces bearing polymer brushes. *Nature* **1994**, *370*, 634.

(4) Lee, S.; Spencer, N. D. Sweet, hairy, soft, and slippery. *Science* **2008**, *319*, 575.

(5) Yu, Y.; Lopez de la Cruz, R. A.; Kieviet, B. D.; Gojzewski, H.; Pons, A.; Vancso, G. J.; de Beer, S. Pick up move and release of nanoparticles utilizing co-non-solvency of PNIPAM brushes. *Nanoscale* **2017**, *9*, 1670−1675.

(6) Cao, Z.; Bian, Q.; Chen, Y.; Liang, F.; Wang, G. Light-Responsive Janus-Particle-Based Coatings for Cell Capture and Release. *ACS Macro Lett.* **2017**, *6*, 1124−1128.

(7) Merlitz, H.; He, G.-L.; Wu, C.-X.; Sommer, J.-U. Nanoscale brushes: How to build a smart surface coating. *Phys. Rev. Lett.* **2009**, *102*, 115702.

(8) Klushin, L. I.; Skvortsov, A. M.; Polotsky, A. A.; Qi, S.; Schmid, F. Sharp and Fast: Sensors and Switches Based on Polymer Brushes with Adsorption-Active Minority Chains. *Phys. Rev. Lett.* **2014**, *113*, No. 068303.

(9) Button, B.; Cai, L.-H.; Ehre, C.; Kesimer, M.; Hill, D. B.; Sheehan, J. K.; Boucher, R. C.; Rubinstein, M. A Periciliary Brush Promotes the Lung Health by Separating the Mucus Layer from Airway Epithelia. *Science* **2012**, *337*, 937−941.

(10) McCaig, H. C.; Myers, E.; Lewis, N. S.; Roukes, M. L. Vapor Sensing Characteristics of Nanoelectromechanical Chemical Sensors Functionalized Using Surface-Initiated Polymerization. *Nano Lett.* **2014**, *14*, 3728−3732.

(11) Yang, H.; Zhu, H.; Hendrix, M. M. R. M.; Lousberg, N. J. H. G. M.; de With, G.; Esteves, A. C. C.; Xin, J. H. Temperature-Triggered Collection and Release of Water from Fogs by a Sponge-Like Cotton Fabric. *Adv. Mater.* **2013**, *25*, 1150−1154.

(12) Liu, X.; Li, Y.; Hu, J.; Jiao, J.; Li, J. Smart moisture management and thermoregulation properties of stimuli-responsive cotton modified with polymer brushes. *RSC Adv.* **2014**, *4*, 63691−63695.

(13) Kobayashi, M.; Terayama, Y.; Hosaka, N.; Kaido, M.; Suzuki, A.; Yamada, N.; Torikai, N.; Ishihara, K.; Takahara, A. *Soft Matter* **2007**, *3*, 740.

(14) de Beer, S.; Kutnyanszky, E.; Schön, P. M.; Vancso, G. J.; Müser, M. H. Solvent induced immiscibility of polymer brushes eliminates dissipation channels. *Nat. Commun.* **2014**, *5*, No. 3781.

(15) Thiele, U.; Hartmann, S. Gradient dynamics model for drops spreading on polymer brushes. *Eur. Phys. J.: Spec. Top.* **2020**, *229*, 1819−1832.

(16) Andreotti, B.; Snoeijer, J. H. Statics and Dynamics of Soft Wetting. *Annu. Rev. Fluid Mech.* **2020**, *52*, 285−308.

(17) Karpitschka, S.; Das, S.; van Gorcum, M.; Perrin, H.; Andreotti, B.; Snoeijer, J. H. Droplets move over viscoelastic substrates by surfing a ridge. *Nat. Commun.* **2015**, No. 12517.

(18) Flory, P. J. *Principles of Polymer Chemistry*; Cornell University Press: Ithaca, 1953.

(19) Laschitsch, A.; Bouchard, C.; Habicht, J.; Schimmel, M.; Rühe, J.; Johannsmann, D. Thickness Dependence of the Solvent-Induced Glass Transition in Polymer Brushes. *Macromolecules* **1999**, *32*, 1244−1251.

(20) Biesalski, M.; Rühe, J. Swelling of a Polyelectrolyte Brush in Humid Air. *Langmuir* **2000**, *16*, 1943−1950.

(21) Galvin, C. J.; Dimitriou, M. D.; Satija, S. K.; Genzer, J. Swelling of Polyelectrolyte and Polyzwitterion Brushes by Humid Vapors. *J. Am. Chem. Soc.* **2014**, *136*, 12737−12745.

(22) Galvin, C. J.; Genzer, J. Swelling of Hydrophilic Polymer Brushes by Water and Alcohol Vapors. *Macromolecules* **2016**, *49*, 4316−4329.

(23) Sun, L.; Akgun, B.; Hu, R.; Browning, J. F.; Wu, D. T.; Foster, M. D. Scaling Behavior and Segment Concentration Profile of Densely Grafted Polymer Brushes Swollen in Vapor. *Langmuir* **2016**, *32*, 5623−5628.

(24) Orski, S. V.; Sheridan, R. J.; Chan, E. P.; Beers, K. L. Utilizing vapor swelling of surface-initiated polymer brushes to develop quantitative measurements of brush thermodynamics and grafting density. *Polymer* **2015**, *72*, 471−478.

(25) Jayachandran, K. N.; Chatterji, P. R.; Pausnitz, J. M. Vapor-Liquid Equilibria for Solutions of Brush Poly(methyl methacrylate) in Chloroform. *Macromolecules* **1998**, *31*, 2375−2377.

(26) Plimpton, S. Fast Parallel Algorithms for Short-Range Molecular Dynamics. *J. Comput. Phys.* **1995**, *117*, 1.

(27) Kremer, K.; Grest, G. S. Dynamics of entangled linear polymer melts: A molecular-dynamics simulation. *J. Chem. Phys.* **1990**, *92*, 5057.

(28) Singh, M. K.; Ilg, P.; Espinosa-Marzal, R. M.; Kröger, M.; Spencer, N. D. Polymer Brushes under Shear: Molecular Dynamics Simulations Compared to Experiments. *Langmuir* **2015**, *31*, 4798−4805.

(29) Klushin, L. I.; Skvortsov, A. M.; Qi, S.; Kreer, T.; Schmid, F. Polydispersity Effects on Interpenetration in Compressed Brushes. *Macromolecules* **2019**, *52*, 1810−1820.

(30) de Vos, W. M.; Leermakers, F. A. M.; de Keizer, A.; Kleijn, J. M.; Cohen Stuart, M. A. Interaction of Particles with a Polydisperse Brush: A Self-Consistent-Field Analysis. *Macromolecules* **2009**, *42*, 5881−5891.

(31) Veldscholte, L. B. MDBrushGenerator, 2020 DOI: 10.5281/zenodo.3944454.

(32) Opferman, M. G.; Coalson, R. D.; Jasnow, D.; Zilman, A. Morphology of Polymer Brushes Infiltrated by Attractive Nano-inclusions of Various Sizes. *Langmuir* **2013**, *29*, 8584−8591.

(33) Galuschko, A.; Sommer, J.-U. Co-Nonsolvency Response of a Polymer Brush: A Molecular Dynamics Study. *Macromolecules* **2019**, *52*, 4120−4130.

(34) Braun, E.; Moosavi, S. M.; Smit, B. Anomalous Effects of Velocity Rescaling Algorithms: The Flying Ice Cube Effect Revisited. *J. Chem. Theory Comput.* **2018**, *14*, 5262−5272.

(35) Veldscholte, L. B. SPiVHB, 2020 DOI: 10.5281/zenodo.3944343.

(36) Tuckerman, M.; Berne, B. J.; Martyna, G. J. Reversible multiple time scale molecular dynamics. *J. Chem. Phys.* **1992**, *97*, 1990−2001.

(37) Williams, D. R. M. Grafted polymers in bad solvents: octopus surface micelles. *J. Phys. II France* **1993**, *3*, 1313−1318.

(38) Veldscholte, L. B. MDBrushGenerator, 2020 DOI: 10.5281/zenodo.3945235.

(39) Mukherji, D.; Marques, C. M.; Kremer, K. Smart Responsive Polymers: Fundamentals and Design Principles. *Annu. Rev. Condens. Matter Phys.* **2020**, *11*, 271−299.

(40) Yang, G.-W.; Wu, G.-P.; Chen, X.; Xiong, S.; Arges, C. G.; Ji, S.; Nealey, P. F.; Lu, X.-B.; Darensbourg, D. J.; Xu, Z.-K. Directed Self-Assembly of Polystyrene-b-poly(propylene carbonate) on Chemical Patterns via Thermal Annealing for Next Generation Lithography. *Nano Lett.* **2017**, *17*, 1233−1239.

(41) Gumerov, R. A.; Rumyantsev, A. M.; Rudov, A. A.; Pich, A.; Richtering, W.; Möller, M.; Potemkin, I. I. Mixing of Two Immiscible Liquids within the Polymer Microgel Adsorbed at Their Interface. *ACS Macro Lett.* **2016**, *5*, 612−616.

(42) Flory, P. J. Thermodynamics of High Polymer Solutions. *J. Chem. Phys.* **1942**, *10*, 51.

(43) Birshtein, T. M.; Lyatskaya, Y. V. Theory of the Collapse-Stretching Transition of a Polymer Brush in a Mixed Solvent. *Macromolecules* **1994**, *27*, 1256−1266.

(44) Alexander, S. Adsorption of chain molecules with a polar head a scaling description. *J. Phys.* **1977**, *38*, 983.

(45) De Gennes, P. Scaling theory of polymer adsorption. *J. Phys.* **1976**, *37*, 1445−1452.

(46) Israelachvili, J. N. *Intermolecular and Surface Forces*; Academic Press, Elsevier: USA, 2011.

(47) Veldscholte, L. B. *Sorption Characteristics for Polymer Brushes in Equilibrium with Solvent Vapors: dataset*, 2020. https://dx.doi.org/10.4121/uuid:f31d3b2b-1a75-43fb-a85e-c4c7e730c329.

(48) Mukherji, D.; Marques, C. M.; Stuehn, T.; Kremer, K. Depleted depletion drives polymer swelling in poor solvent mixtures. *Nat. Commun.* **2017**, No. 1374.

(49) Opferman, M. G.; Coalson, R. D.; Jasnow, D.; Zilman, A. Morphological control of grafted polymer films via attraction to small nanoparticle inclusions. *Phys. Rev. E* **2012**, *86*, No. 031806.

(50) Brió Pérez, M.; Cirelli, M.; de Beer, S. Degrafting of Brushes by Exposure to Humid Air. *ACS Appl. Polym. Mater.* **2020**, *2*, 3039−3043.

(51) Milner, S. T.; Witten, T. A.; Cates, M. E. Theory of the grafted polymer brush. *Macromolecules* **1988**, *21*, 2610.

(52) Klein, J. Hydration lubrication. *Friction* **2013**, *1*, 1−23.

(53) Cohen Stuart, M. A.; de Vos, W. M.; Leermakers, F. A. M. Why Surfaces Modified by Flexible Polymers Often Have a Finite Contact Angle for Good Solvents. *Langmuir* **2006**, *22*, 1722−1728.

(54) Maas, J. H.; Fleer, G. J.; Leermakers, F. A. M.; Cohen Stuart, M. A. Wetting of a Polymer Brush by a Chemically Identical Polymer Melt: Phase Diagram and Film Stability. *Langmuir* **2002**, *18*, 8871−8880.

(55) Pastorino, C.; Binder, K.; Kreer, T.; Müller, M. Static and dynamic properties of the interface between a polymer brush and a melt of identical chains. *J. Chem. Phys.* **2006**, *124*, No. 064902.

(56) Mensink, L. I. S.; Snoeijer, J. H.; de Beer, S. Wetting of Polymer Brushes by Polymeric Nanodroplets. *Macromolecules* **2019**, *52*, 2015−2020.

(57) Zhang, W.; Gomez, E. D.; Milner, S. T. Predicting Flory-Huggins χ from Simulations. *Phys. Rev. Lett.* **2017**, *119*, No. 017801.

(58) Rodrıguez, O.; Fornasiero, F.; Arce, A.; Radke, C. J.; Prausnitz, J. M. Solubilities and diffusivities of water vapor in poly(methylmethacrylate), poly(2-hydroxyethylmethacrylate), poly(N-vinyl-2-pyrrolidone) and poly(acrylonitrile). *Polymer* **2003**, *44*, 6323−6333.

(59) Milczewska, K.; Voelkel, A.; Piędzia, K. Interactions in PEG/Aerosil and PLA/Aerosil composites described by IGC-determined Flory-Huggins χ_{23} parameter. *J. Polym. Res.* **2014**, *21*.